Novel Design of a Nanoflowmeter Based on Carbon Nanotubes

DATASET *in* THE JOURNAL OF PHYSICAL CHEMISTRY C · JUNE 2012

Impact Factor: 4.77 · DOI: 10.1021/jp302895a

3 AUTHORS:

Lina Zhao
Institute of High Energy Physics (Chinese Acad…
62 PUBLICATIONS **710** CITATIONS
SEE PROFILE

Yuliang Zhao
Chinese Academy of Sciences
345 PUBLICATIONS **12,009** CITATIONS
SEE PROFILE

Zhou Ruhong
IBM
133 PUBLICATIONS **5,912** CITATIONS
SEE PROFILE

THE JOURNAL OF PHYSICAL CHEMISTRY C

Article

pubs.acs.org/JPCC

Novel Design of a Nanoflowmeter Based on Carbon Nanotubes

Lina Zhao,[†] Yuliang Zhao,*[,†,‡] and Ruhong Zhou*[,§,∥]

[†]CAS Key Laboratory for Biomedical Effects of Nanomaterials and Nanosafety, Institute of High Energy Physics, Chinese Academy of Sciences (CAS), Beijing 100049, China

[‡]National Center for Nanoscience and Technology of China, Beijing 100190, China

[§]Computational Biology Center, IBM Thomas J. Watson Research Center, Yorktown Heights, New York 10598, United States

[∥]Department of Chemistry, Columbia University, New York, New York 10027, United States

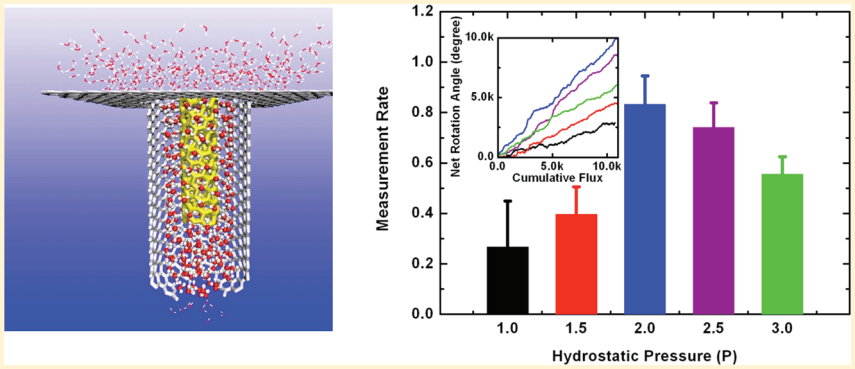

ABSTRACT: The ultimate goal of nanotechnology is to construct integrated complex nanosystems with various functions. To achieve this goal, one must first establish solid, yet simple, nanounits (or nanoparts) such as nanomotors and nanoflowmeters. In this work, we computationally designed a novel nanoflowmeter based on two carbon nanotubes, with a smaller inner chiral tube as the "rotator" and a larger outer tube as the "stator" (or container), to measure the fluid flow between the two nanotubes. We found that the water nanoflowmeter could be gauged by the unidirectional motion of the chiral nanorotator even under severe thermal fluctuations at the nanoscale. The nanoflowmeter exhibited an excellent correlation between the cumulative net flux of water and the net rotation angle, which served as the underlying mechanism for our nanoflowmeter measurements. We then further optimized the design of the nanoflowmeter by introducing partial charges onto the inner rotator with "screwlike patterns" to enhance the chirality. The concerted motion of the water molecules could then be modulated by these partial charges, which direct the dipole orientation of water molecules and form a tailored configuration of a hydrogen-bond network in nanoconfinement. The present findings from molecular modeling could provide the foundation for a more sophisticated and practical nanoflowmeter.

INTRODUCTION

Fluid flows are of critical importance to the structure and function of biomolecules.[1−4] It is essential to quantify the transport of these flowing fluids at the nanoscale[5] in both biological microenvironments and nanotechnological applications. Some previous electrometric efforts were devoted toward this challenge. For example, single-walled carbon nanotubes (SWNTs) and bundles thereof have been utilized to detect the ionic conductivity of the surrounding liquid flow by the induced voltage.[6−8] Multilayers of gold nanoparticles have been assembled to sense the polar liquids flowing through them.[9] However, these flow sensors are effective only on ionic flows[6−9] for electric measurements, and their sizes are still on the order of micrometers to millimeters and beyond.[6,7,9,10]

Despite these recent efforts, the critical question still remains: How can one achieve a general fluid flow measurement at the nanoscale? Constructing a practical molecular nanomachine offers a logical first step.[11] Particular attention has been directed toward artificial nanostructures that can potentially exhibit internal unidirectional rotation, rather than random flipping in either direction.[12] This internal unidirectional rotation is the pillar of the design of all molecular machines, which work just like their macroscale counterparts.[13] Molecular rotors are one major area of study among various types of molecular nanomachinery. Recently, the Michl group designed several surface-mounted molecular rotors, including azimuthal and altitudinal rotors, driven by rotating electric fields,[14,15] linearly oscillating fields,[16,17] light,[18] and fluid flow.[19] Tour and coworkers assembled complex molecules into nanocars and nanodragsters with directional control,[20,21] in which the C_{60} wheels were thermally decoupled from the solid surface so that they could rotate freely.[22,23] The Král group reported rolling nanorods on the surface of water that were driven Coulombically.[24] For all of these investigations of rotors either mounted

Received: March 26, 2012
Revised: May 8, 2012
Published: May 11, 2012

   dx.doi.org/10.1021/jp302895a | J. Phys. Chem. C 2012, 116, 13429−13434

on surface rigidly, or rotating on surface freely, the aim was to utilize opposite[14−19] or direct[20−24] rotational motions to transport nanoscale cargo in microfluidic channels. However, accurately measuring fluid flow in such designs is difficult. Another important category of molecular rotors is generated in solution,[12,25] offering the advantage of sensing the surrounding fluid flows. The Kelly group synthesized complex organic structures and achieved 120° unidirectional motion coupled with a chemical reaction to supply energy.[26,27] The Feringa group produced 360° unidirectional motion around a double bond of an organic structure in solution.[28,29] So far, almost all molecular rotors designed for the solution or vapor phase have used various freely floating organic structures with complex components, which might have difficulty in responding to fluid flow in an accurately measurable way.[12,18]

Fortunately, carbon nanotubes (CNTs) appear to be promising candidates for objects that can move regularly and periodically in response to different external fields,[30,31] because of their unique geometrical stability and elastic properties.[32,33] Molecular bearings based on multiwalled carbon nanotubes (MWNTs) using the relative sliding and rotation motions between neighboring walls have been proposed theoretically.[30,31,34,35] However, is it possible to construct effective measurement devices from CNTs immersed in fluid flows? Can a molecular flowmeter establish a consistent measuring gauge? In this study, we proposed a novel nanoflowmeter based on a dual-carbon nanotube (D-CNT) system to meet these challenges. As a prototype for other liquid or gas flow measurements at the molecular level, we considered water molecules as the medium in the present study. SWNTs have been designed as molecular channels for water molecules.[36−38] Furthermore, water transportation gating control[39] and water-mediated signal multiplication[40] have been proposed computationally.[41,42] In the current study, we computationally designed a water nanoflowmeter with an idealized model D-CNT system (a chiral inner CNT small enough to have no water flow inside and an outer CNT large enough to have water flow between the two nanotube walls) with molecular dynamics (MD) simulations and found an excellent correlation between the cumulative net flux of water and the net rotation angle, which serves as the underlying mechanism for nanoflowmeter measurements. Moreover, the measurement mechanism was optimized further by decorating the chiral rotator with partial charges in "screwlike patterns". We expect the device to work well in other fluids with other dimensions of nanotubes as well, as long as there are net flows between the two nanotubes. The designed water nanoflowmeter and its derivatives for other fluid flows should be of importance for bioactivity and nanotechnological applications to achieve accurate nanoflow measurements under nanoconfinement full of thermal fluctuations.

MODEL AND METHOD

For simplicity, we used water molecules as the sample for measurement in this study. Figure 1 shows the molecular configuration of the water nanoflowmeter, along with a schematic drawing of a macroscopic flowmeter. The D-CNT system of the water nanoflowmeter consisted of an uncapped chiral (6,3)-CNT with a diameter of 6.2 Å and a length of 25.0 Å as the inner rotator surrounded coaxially by a one-end-capped armchair (14,14)-CNT with a diameter of 19.0 Å and a length of 40.0 Å as the outer stator. The uncapped end of the (14,14)-CNT stator was "anchored" with a graphene sheet in

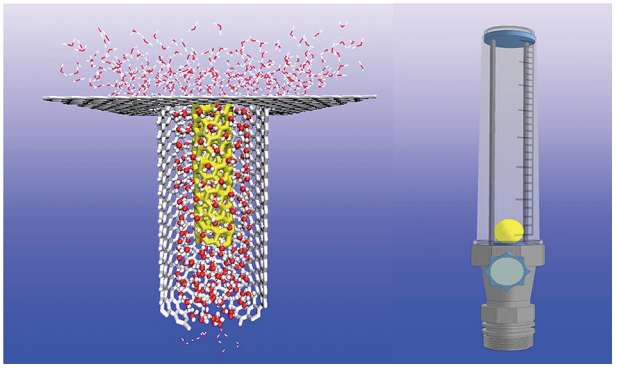

Figure 1. Molecular configuration of the dual-carbon nanotube (D-CNT) system as the water nanoflowmeter, along with a schematic drawing of a macroscopic flowmeter (on the right). The system consists of a coaxial arrangement of an uncapped chiral (6,3)-CNT (yellow, diameter = 6.2 Å) with a length of 25.0 Å as the inner rotator and a one-end-capped armchair (14,14)-CNT with a length of 40.0 Å as the outer stator (white, diameter = 19.0 Å). Water molecules are depicted with oxygen in red and hydrogen in white, in the CPK representation inside the nanoflowmeter and lines outside it. The water molecules outside the (14,14)-CNT and beneath the graphene sheet (white) are not shown for clarity.

contact with a water reservoir, which was used as the entrance of the water flow for measurement. In the directional water stream system, the hydrostatic pressure was applied on the water molecules in the $+Z$ direction along the axis of the D-CNT. On the other, capped end of the (14,14)-CNT stator, one nanohole with a diameter of 9.0 Å was introduced for water disposal. More importantly, the relatively small hole decreased the speed of water flow and accumulated water molecules in the space below the (6,3)-CNT rotator, which provided enough buoyancy for the rotator to keep its proper floating position, as shown in the molecular configuration as Figure 1. To mimic this floating effect in our MD simulations, we constrained the (6,3)-CNT rotator loosely in the Z direction by using harmonic constraint method with a force constant of 0.6 kcal/(mol Å^2). No water flowed through the floating (6,3)-CNT rotator because of its small diameter, whereas a cylindrical monolayer of water formed between the two nanotubes. For the current design, there was no restrictive requirement on the exact sizes of the two nanotubes, as long as no water (or other liquids) flowed in the inner tube but sufficient water flowed in the gap region. The water flow inside the nanoconfinement (gap region) could drive the chiral (6,3)-CNT rotator to rotate unidirectionally under a certain hydrostatic pressure.

We used molecular dynamics (MD) simulations to model the designed D-CNT system with the NAMD2 package (NAMD v2.6). MD simulations have been widely used in the studies of both biomolecules[43−47] and nanomaterials.[48−50] For this D-CNT water measurement system, the TIP3P water model was used. The interactions between the carbon atoms of the nanoflowmeter and the measured water molecules were generated using the CHARMM27 force field. Carbon atoms were assumed to be of type CA with Lennard-Jones parameters ε_{cc} = −0.0700 kcal/mol and $R_{min}/2$ = 1.9924 Å. Langevin dynamics was employed to control the temperature at a constant 300 K. The particle-mesh Ewald (PME) method was employed for the long-range electrostatic interactions. The smooth cutoff of the short-range van der Waals interactions was set at 12 Å. A time step of 2 fs was used, and the data were collected every 1 ps. We applied periodic boundary conditions

dx.doi.org/10.1021/jp302895a | J. Phys. Chem. C 2012, 116, 13429−13434

in all directions. After energy minimization, the water nanoflowmeter system was equilibrated for 5 ns within the *NPT* ensemble (T = 300 K, P = 1 atm) using the Nosé–Hoover Langevin piston method. The production runs were carried out in the *NVT* ensemble at a constant temperature of 300 K and in a constant volume of 39.0 × 39.0 × 105.0 Å^3 with ∼11300 atoms. We simulated the gauge relationships of the pristine nanoflowmeter under hydrostatic pressures of 1.0P, 1.5P, 2.0P, 2.5P, and 3.0P (1P = 103.2 MPa). Furthermore, we decorated partial charges on the (6,3)-CNT rotator with different screwlike patterns to enhance the "chirality" (or asymmetry) for the optimal performance of the water nanoflowmeter, with partial charge magnitudes of ±0.0625e, ±0.125e, ±0.25e, ±0.375e, and ±0.625e for "armchair decoration" (AD) and ±0.05e, ±0.10e, ±0.20e, ±0.30e, and ±0.50e for "zigzag decoration" (ZD) (see Figure 4 below). More importantly, these partial charges can be used to help detect nanorotation through the periodic electric fields generated by the rotating partial charges. A total of 25 trajectories, of 60 ns each, were performed for the water nanoflowmeter study under different hydrostatic pressures, as well as various screwlike patterns of partial charges.

RESULTS AND DISCUSSION

We found that water molecules can transport through the D-CNT system at a stable transportation velocity under a certain hydrostatic pressure. As shown in Figure 2A, under a hydrostatic pressure of 2.0P, for example, the cumulative flux of water grew almost linearly with simulation time at a transportation velocity of 360.7 molecules/ns. During simulations of the water transportation dynamics, it was remarkable to find that the inner chiral (6,3)-CNT rotator rotated continuously and unidirectionally, driven by the water flow between the two nanotubes. A cylindrical monolayer of hydrogen-bonded (H-bond) water molecules was found in the nanoconfined gap region. This cylindrical monolayer water network interacted with the (6,3)-CNT rotator and pushed it to rotate unidirectionally. As shown in the top-view inset in Figure 2B, the screwlike pattern in the chiral structure transferred the axial pressure from the water flow into an axial-perpendicular unidirectional net driving force. As shown in Figure 2B, the net rotation angle θ of the inner rotator increased monotonically with the simulation time at an average rotation rate of around 289.1°/ns, even though it did rotate back and forth from time to time in a small range (only several degrees) because of thermal fluctuations. As a result, a direct relationship was found between the cumulative net flux of water and the net rotation angle in the D-CNT system, which is the underlying mechanism of our nanoflowmeter (more details are presented in Figure 3B, below).

To monitor the quantitative gauge of the water nanoflowmeter with different transportation velocities, we calculated the cumulative flux of water and rotation properties of the nanoflowmeter under hydrostatic pressures of 1.0P, 1.5P, 2.0P, 2.5P, and 3.0P. The cumulative flux of water increased as the hydrostatic pressure increases from 1.0P to 3.0P, as indicated in Figure 3A. Moreover, the transportation velocities of water could be controlled linearly by increasing the hydrostatic pressure, with the changes in the water cumulative flux being in direct proportion to the changes in the hydrostatic pressure. The inset of Figure 3B shows a plot of the direct measurement relationship between the cumulative flux of water and the net rotation angle of rotator at various hydrostatic pressures, that is,

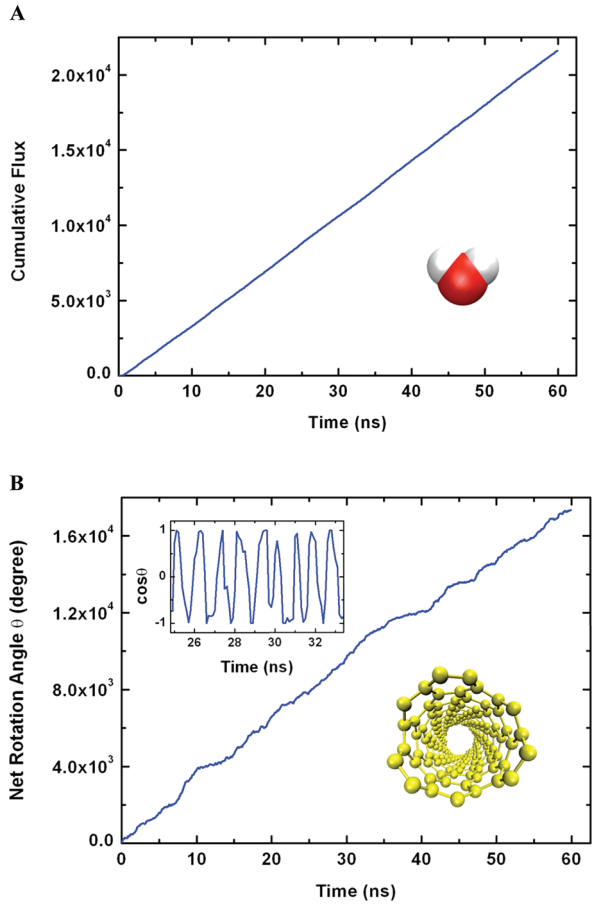

Figure 2. (A) Cumulative flux of the measured water molecules and (B) net rotation angle θ of the (6,3)-CNT rotator as functions of the simulation time in the water nanoflowmeter under a hydrostatic pressure of 2.0P. Inset in A: Sketch of the measured water molecule. Insets in B: (top) Plot of cos θ versus simulation time and (bottom) sketch of a top view of the (6,3)-CNT rotator.

various transportation velocities of water. These linear relationships offer a straightforward gauge rule. We defined the slopes of the monotonic relationships as the measurement rates of the water nanoflowmeter, which measures the corresponding magnitude of the degrees of rotation driven by a unit of permeating water molecules. As shown in Figure 3B, the measurement rate increased with increasing hydrostatic pressure until reaching a maximum value of around 0.8°/molecule at 2.0P; then it decreased slightly as the hydrostatic pressure continued to increase. In the current design of the nanoflowmeter, there appeared to be two operating regimes: hydrostatic pressure < 2.0P and hydrostatic pressure > 2.0P. In the first regime, the external pressure has no significant influence on the effect of water floating the rotator, and the rotator works optimally within its constraints in the Z direction (the "optimal constrained" mode). All transporting water molecules effectively drive the rotator only in the X–Y plane, so the measurement rate increases with the water transportation velocity until ∼2.0P. When the hydrostatic pressure becomes too large in the second regime, it overcomes the buoyancy on the rotator and pushes the rotator out of the optimal constrained mode. Part of the net water flow driving force in this case is dissipated in rotator oscillations in all directions, including the Z direction, causing a reduction in the net torque for unidirectional rotation. In other words, there seems to be an

dx.doi.org/10.1021/jp302895a | J. Phys. Chem. C 2012, 116, 13429–13434

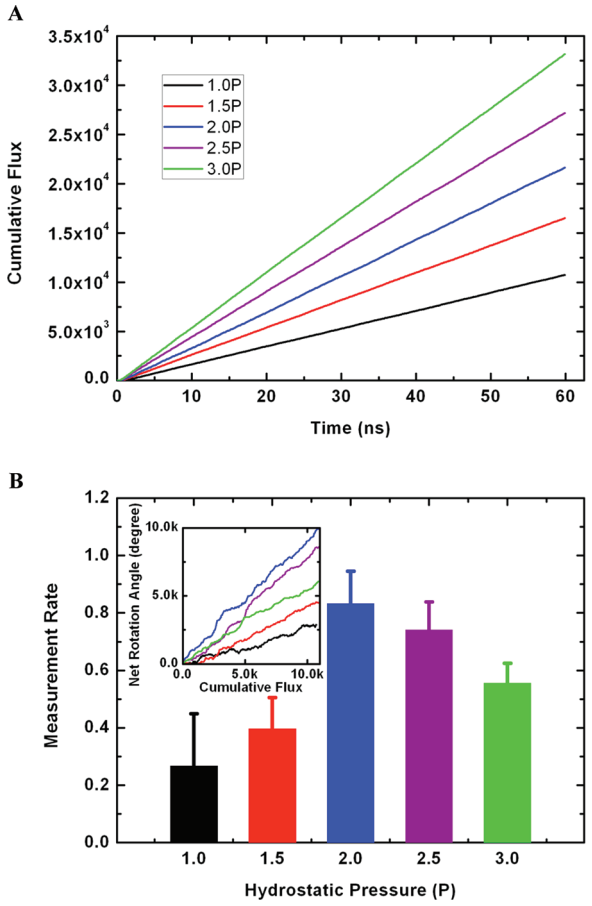

Figure 3. (A) Cumulative flux of the measured water molecules as a function of the simulation time in the water nanoflowmeter under different hydrostatic pressures: 1.0P (black), 1.5P (red), 2.0P (blue), 2.5P (purple), and 3.0P (green). (B) Measurement rates of the water nanoflowmeter under different hydrostatic pressures. Inset in B: Direct measurement relationship between the net rotation angle of the (6,3)-CNT rotator and the cumulative flux of the measured water molecules for different hydrostatic pressures. The slopes of these relationships are defined as the measurement rates of the device.

optimal water flow speed (and thus an optimal hydrostatic pressure) for net rotator unidirectional rotation. In the current design, the water nanoflowmeter performed most effectively under a hydrostatic pressure of ~2.0P.

In addition, the error bars of the flow measurement rates describe another useful unidirectional property of the nanoflowmeter, namely, the rotational sensitivity. The rotational sensitivity increased with increasing hydrostatic pressure (see the error bars for 1.0P and 3.0P in Figure 3B).

Overall, the measured angle rotation rate is the intrinsic parameter of the D-CNT system to gauge its function as a nanoflowmeter. The cumulative net flux can be measured by reading the rotation angle directly. So far, the models of the water nanoflowmeter that we studied were all pristine D-CNT systems. However, the transport of water can be further influenced by nearby external charges, because of water's asymmetric charge distribution, especially under nanoscale confinement.[39,40] Meanwhile, the gauge rotation of the nanoflowmeter is supported by the asymmetric chiral structure of the (6,3)-CNT, which, of course, can be further modulated. To put these two key points together, we decorated the inner (6,3)-CNT rotator with partial charges in screwlike patterns to optimize the nanoflowmeter performance. We designed two screwlike patterns for partial charge decorations, defined as armchair decoration (AD) and zigzag decoration (ZD), to enhance the chirality based on the original screwlike structure of the chiral rotator. The names of armchair decoration (AD) and zigzag decoration (ZD) arise from the shape along the partial charge "screw line", as the configurations for AD and ZD depicted at the left and right, respectively, of Figure 4. For AD,

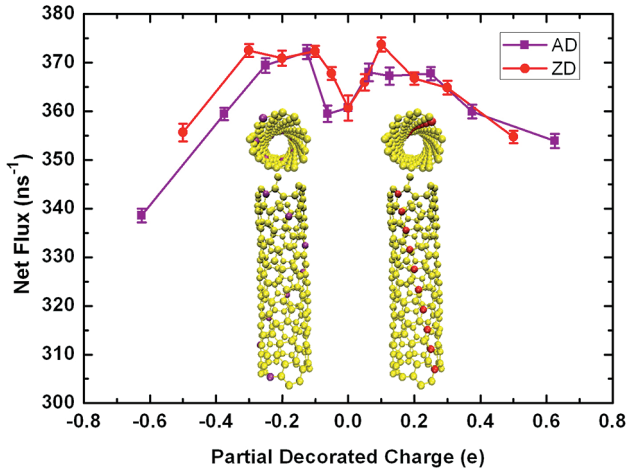

Figure 4. Net flux with respect to different screwlike decorated partial charges for armchair decoration (AD) and zigzag decoration (ZD). Inset: Configuration of the (6,3)-CNT rotator in D-CNT nanoflowmeter measurements with screwlike partial charge decoration. Left: Top and side views of armchair decoration with eight decorated partial charges in purple. Right: Top and side views of zigzag decoration with 10 decorated partial charges in red.

on the hexagonal lattice, the partial charges are decorated on one C atom from one end of the (6,3)-CNT rotator and then the para position C atom from the current C atom's ortho position (see Figure 4) and follow the same decoration pattern to the other end of rotator, where the armchair pattern can be achieved along the decoration screw line. For ZD, the partial charges are decorated on the meta position carbon atoms from one end to the other end of the (6,3)-CNT rotator, presenting a zigzag pattern along the decoration screw line. For AD, eight partial charges make up one complete circle, with an exact 360° "screw angle" along the 25.0-Å length of the (6,3)-CNT rotator. (See the top and side views with the decorated partial charges in purple.) For ZD, 10 partial charges make up a 77.42° screw angle, where the decorated partial charges are colored in red. To achieve the optimized performance of the nanoflowmeter under AD and ZD, the partial charge magnitudes were varied, with values of ±0.0625e, ±0.125e, ±0.25e, ±0.375e, and ±0.625e for AD and values of ±0.05e, ±0.10e, ±0.20e, ±0.30e, and ±0.50e for ZD, to have equal total charges in each case for AD and ZD. In Figure 4, the profiles of the water net flux in the nanoflowmeter versus the partial charges decorated on the (6,3)-CNT rotator are shown in a purple line with square marks and a red line with circle marks for AD and ZD, respectively. The overall water transport of the nanoflowmeter with the ZD pattern is slightly better than that of the nanoflowmeter with the AD pattern, in which the decorated nanoflowmeter reached its most optimized transport performance with a partial charge of +0.10e. When the absolute magnitudes of the partial charges increased, for both AD and

dx.doi.org/10.1021/jp302895a | J. Phys. Chem. C 2012, 116, 13429−13434

ZD, the water net flux first increased and then decreased until it was even smaller than that of the pristine rotator.

To understand the underlying mechanism for the optimization of the nanoflowmeter transportation, we analyzed the detailed configurations and dipole orientations of water molecules influenced by the decoration patterns and magnitudes of partial charges on the (6,3)-CNT rotator in Figure 5. We chose the ZD pattern with +0.10e partial charges

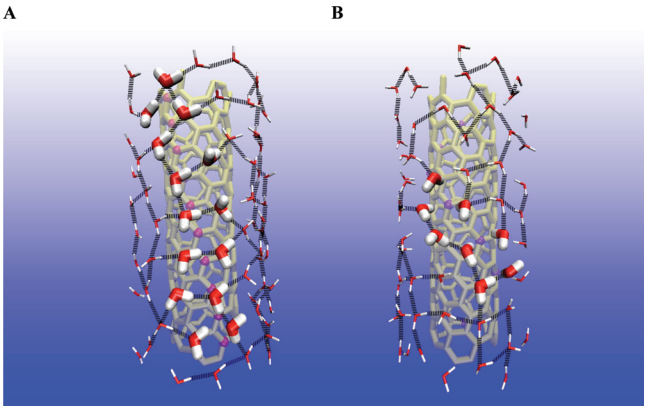

Figure 5. Molecular configurations of monolayer cylindrical water with H-bond networks between the (6,3)-CNT rotator and the (14,14)-CNT stator of the nanoflowmeter for (A) zigzag decoration (ZD) with +0.10e partial charge and (B) armchair decoration (AD) with −0.625e partial charge. The snapshots were taken around 35 ns into the 60-ns trajectories. The water molecules are described in LICORICE representation with oxygen in red and hydrogen in white. The water molecules near the partial charges on the rotator are highlighted with a larger radius (0.4 Å), and others are shown with a smaller radius (0.1 Å). The H-bonds are presented as thick black lines. The water molecules in the lower half of the cylindrical monolayer are hidden for display purposes. The (6,3)-CNT rotator in yellow is shown as transparent for the clarity of water network configurations. The depiction of the partial charges in (A) red (ZD, +0.10e) and (B) purple (AD, −0.625e) is consistent with the colors used in the inset of Figure 4.

and the AD pattern with −0.625e partial charges as the typical case studies, which modulated the water transport into the maximum and minimum net fluxes, respectively, as implied in Figure 4. As noted above, for the screwlike ZD (Figure 5A) and AD (Figure 5B) patterns, the partial charges were distribute within only 77.42° on the (6,3)-CNT rotator in the ZD pattern, whereas the partial charges were distributed evenly around one complete circle along the axis in the AD pattern. Thus, the partial charges in the ZD pattern introduced more asymmetry into the nanoflowmeter than those in the AD pattern and were thus better able to control and optimize the transport performance of the nanoflowmeter. Second, the positive and negative electrical properties of the partial charges directed the water molecules into different dipole orientations. As shown in Figure 5, the oxygen atoms of the water molecules are pointed toward the rotator's neighboring positive partial charges (+0.10e) in Figure 5A (best case). By contrast, the hydrogens of the water molecules are pointed toward the rotator's neighboring negative partial charges (−0.625e) in Figure 5B (worst case). Third, the magnitudes of partial charges were able to control the water transportation sensitively, which can be seen from the water configurations and H-bond networks in Figure 5 (where the O···O distance and the O−H···O angle for a H-bond are defined as 3.5 Å and 150°, respectively). When the partial charges were introduced onto the rotator, the probability distributions of the dipole orientations and configurations of the monolayer water molecules were ordered with higher degrees, as the absolute magnitudes of partial charges increased gradually from zero. The ordered configurations of water molecules formed H-bonds between water molecules, resulting in a stronger H-bond network. As shown in Figure 5A, when the partial charges in the ZD pattern had a value of +0.10e, the ordered H-bond network promoted the concerted motion of water molecules distributed on the confined cylindrical surface, and the net flux accelerated to reach a maximum value for the nanoflowmeter. By contrast, when the absolute magnitudes of the partial charges increase further, the stronger electrostatic attractions from the partial charges started to "lock" nearby water molecules near the partial charges and thus disturbed the H-bonded water network configurations. In other words, the H−O bonds of water molecules deviated from being roughly parallel to the cylindrical surface of the H-bond network (shown in Figure 5A) into being more vertical with respect to the H-bond network (shown in Figure 5B). Moreover, the H-bonds between the water molecules along the decoration screw line were broken because of the distortions of water configurations, as shown in Figure 5B. This suggests that the collective effect of the H-bond network was impaired and that the concerted motion of water molecules decreased accordingly. Moreover, this led to a stronger viscous friction between water molecules and the rotator by the "rough" cylindrical monolayer water network with vertical H−O bonds to the transportation channel. Therefore, the magnitudes of partial charges modulated the transportation behavior of the nanoflowmeter in a parabola-like manner within the negative or positive partial charge region (displaying a "gull-wing" diagram, as shown in Figure 4).

In addition, another benefit for decorating partial charges is that one could, in principle, read the rotation angle of the (6,3)-CNT rotator by detecting the periodic electric fields generated from these partial charges, which could help create practical detection methods for the output signal of the nanoflowmeter.

■ CONCLUSION

In summary, we have designed a novel nanoflowmeter with the unidirectional rotation of an inner chiral nanorotator inside a larger nanotube through water permeation under hydrostatic pressure. For the current design with coaxial (6,3)-CNT and (14,14)-CNT, one monolayer of a cylindrical H-bonded water network is formed between the two nanotubes, which causes the inner rotator to rotate unidirectionally and linearly with the net water flux under hydrostatic pressures. We then further optimized the nanoflowmeter performance by introducing partial charges onto the inner rotator in screwlike patterns to enhance the chirality and asymmetry. The partial charges in a zigzag pattern (ZD) introduced more asymmetry into the rotator than those in an armchair pattern (AD) based on its original chiral structure. Thus, the overall water transport of the nanoflowmeter in the ZD pattern was better than that of the nanoflowmeter in the AD pattern, with the former decorated nanoflowmeter reaching its optimal transportation performance with a partial charge of +0.10e. Together with the screwlike structures, the different electrical properties could direct the water dipole orientation into various configuration patterns and H-bond networks. Accordingly, the concerted motion of water molecules can be modulated by these partial charges, which

dx.doi.org/10.1021/jp302895a | J. Phys. Chem. C 2012, 116, 13429−13434

direct the dipole orientation of water molecules and form a tailored hydrogen-bond network configuration under nanoconfinement. Furthermore, the periodic electric fields generated by the decorated partial charges could help in the design of a practical detection method for the output signal of our nanoflowmeter. Although this study was is based on a nanoflowmeter for water, the method and design can be extended to other fluids, particularly polar ones. The current prototype investigation not only establishes guidelines for experimental fabrications of water flowmeters, but also provides insight into the design of other important liquid and gas flowmeters for diverse applications of nanotechnologies.

AUTHOR INFORMATION

Corresponding Author

*E-mail: ruhongz@us.ibm.com (R.Z). E-mail: zhaoyuliang@ihep.ac.cn (Y.Z.).

Notes

The authors declare no competing financial interest.

ACKNOWLEDGMENTS

This work was supported by the 973 program (2011CB933400, 2010CB933904, and 2010CB933600); the CAS Knowledge Innovation Program, Scientific Research Foundation for Returned Overseas Chinese Scholars, Ministry of Education (1Z201011740329); and the Scientific and Technological Activities Preferred Foundation for Overseas Scholars, Ministry of Personnel (1I20094160283). R.Z. acknowledges support from the IBM Blue Gene Science program.

REFERENCES

(1) Miyazawa, A.; Fujiyoshi, Y.; Unwin, N. *Nature* **2003**, *423*, 949−955.
(2) Denker, B. M.; Smith, B. L.; Kuhajda, F. P.; Agre, P. *J. Biol. Chem.* **1988**, *263*, 15634−15642.
(3) Nelson, D. L.; Cox, M. M. *Lehninger Principles of Biochemistry*; W.H. Freeman: New York, 2008.
(4) Reddy, G.; Straub, J. E.; Thirumalai, D. *Proc. Natl. Acad. Sci. U.S.A.* **2010**, *107*, 21459−21464.
(5) Wang, B.; Král, P. *Phys. Rev. Lett.* **2007**, *98*, 266102.
(6) Král, P.; Shapiro, M. *Phys. Rev. Lett.* **2001**, *86*, 131.
(7) Ghosh, S.; Sood, A.; Kumar, N. *Science* **2003**, *299*, 1042.
(8) Bourlon, B.; Wong, J.; Miko, C.; Forro, L.; Bockrath, M. *Nat. Nanotechnol.* **2007**, *2*, 104−107.
(9) Subramaniam, C.; Pradeep, T.; Chakrabarti, J. *Phys. Rev. Lett.* **2005**, *95*, 164501.
(10) Sood, A.; Ghosh, S. *Phys. Rev. Lett.* **2004**, *93*, 86601.
(11) Michl, J.; Sykes, E. C. H. *ACS Nano* **2009**, *3*, 1042−1048.
(12) Kottas, G. S.; Clarke, L. I.; Horinek, D.; Michl, J. *Chem. Rev.* **2005**, *105*, 1281−1376.
(13) Astumian, R. D. *Science* **1997**, *276*, 917.
(14) Vacek, J.; Michl, J. *Proc. Natl. Acad. Sci. U.S.A.* **2001**, *98*, 5481.
(15) Horinek, D.; Michl, J. *J. Am. Chem. Soc.* **2003**, *125*, 11900−11910.
(16) Horinek, D.; Michl, J. *Proc. Natl. Acad. Sci. U.S.A.* **2005**, *102*, 14175.
(17) Zheng, X.; Mulcahy, M. E.; Horinek, D.; Galeotti, F.; Magnera, T. F.; Michl, J. *J. Am. Chem. Soc.* **2004**, *126*, 4540−4542.
(18) Vacek, J.; Michl, J. *Adv. Funct. Mater.* **2007**, *17*, 730−739.
(19) Vacek, J.; Michl, J. *New J. Chem.* **1997**, *21*, 1259−1268.
(20) Shirai, Y.; Osgood, A. J.; Zhao, Y.; Kelly, K. F.; James, M. *Nano Lett.* **2005**, *5*, 2330−2334.
(21) Vives, G.; Kang, J. H.; Kelly, K. F.; Tour, J. M. *Org. Lett.* **2009**, *11*, 5602−5605.
(22) Akimov, A. V.; Nemukhin, A. V.; Moskovsky, A. A.; Kolomeisky, A. B.; Tour, J. M. *J. Chem. Theory Comput.* **2008**, *4*, 652−656.
(23) Khatua, S.; Guerrero, J. M.; Claytor, K.; Vives, G.; Kolomeisky, A. B.; Tour, J. M.; Link, S. *ACS Nano* **2009**, *3*, 351−356.
(24) Vukovi, L.; Král, P. *Phys. Rev. Lett.* **2009**, *103*, 246103.
(25) Kay, E. R.; Leigh, D. A.; Zerbetto, F. *Angew. Chem., Int. Ed.* **2007**, *46*, 72−191.
(26) Kelly, T. R.; Silva, R. A.; Silva, H. D.; Jasmin, S.; Zhao, Y. *J. Am. Chem. Soc.* **2000**, *122*, 6935−6949.
(27) Kelly, T. R.; De Silva, H.; Silva, R. A. *Nature* **1999**, *401*, 150−152.
(28) Feringa, B. L. *Acc. Chem. Res.* **2001**, *34*, 504−513.
(29) Koumura, N.; Zijlstra, R. W. J.; Van Delden, R. A.; Harada, N.; Feringa, B. L. *Nature* **1999**, *401*, 152−155.
(30) Tuzun, R. E.; Noid, D. W.; Sumpter, B. G. *Nanotechnology* **1995**, *6*, 52.
(31) Tu, Z.; Ou-Yang, Z. *J. Phys.: Condens. Matter* **2004**, *16*, 1287.
(32) Iijima, S. *Nature* **1991**, *354*, 56−58.
(33) Poncharal, P.; Wang, Z. L.; Ugarte, D.; de Heer, W. A. *Science* **1999**, *283*, 1513−1516.
(34) Sohlberg, K.; Tuzun, R. E.; Sumpter, B. G.; Noid, D. W. *Nanotechnology* **1997**, *8*, 103.
(35) Lozovik, Y. E.; Minogin, A. V.; Popov, A. M. *Phys. Lett. A* **2003**, *313*, 112−121.
(36) Hummer, G.; Rasaiah, J. C.; Noworyta, J. P. *Nature* **2001**, *414*, 188−190.
(37) Kalra, A.; Garde, S.; Hummer, G. *Proc. Natl. Acad. Sci. U.S.A.* **2003**, *100*, 10175.
(38) Wan, R.; Lu, H.; Li, J.; Bao, J.; Hu, J.; Fang, H. *Phys. Chem. Chem. Phys.* **2009**, *11*, 9898−9902.
(39) Li, J.; Gong, X.; Lu, H.; Li, D.; Fang, H.; Zhou, R. *Proc. Natl. Acad. Sci. U.S.A.* **2007**, *104*, 3687.
(40) Tu, Y.; Xiu, P.; Wan, R.; Hu, J.; Zhou, R.; Fang, H. *Proc. Natl. Acad. Sci. U.S.A.* **2009**, *106*, 18120.
(41) Zheng, L.; Chen, M.; Yang, W. *Proc. Natl. Acad. Sci. U.S.A.* **2008**, *105*, 20227−20232.
(42) Itoh, S. G.; Tamura, A.; Okamoto, Y. *J. Chem. Theory Comput.* **2010**, *6*, 979−983.
(43) Ge, C.; Du, J.; Zhao, L.; Wang, L.; Liu, Y.; Li, D.; Yang, Y.; Zhou, R.; Zhao, Y.; Chai, Z.; Chen, C. *Proc. Natl. Acad. Sci. U.S.A.* **2011**, *108*, 16968−16973.
(44) Zhou, R.; Huang, X.; Margulis, C. J.; Berne, B. J. *Science* **2004**, *305*, 1605−1609.
(45) Eleftheriou, M.; Germain, R. S.; Royyuru, A. K.; Zhou, R. *J. Am. Chem. Soc.* **2006**, *128*, 13388−13395.
(46) Hua, L.; Huang, X.; Liu, P.; Zhou, R.; Berne, B. J. *J. Phys. Chem. B* **2007**, *111*, 9069−9077.
(47) Huang, X.; Hagen, M.; Kim, B.; Friesner, R. A.; Zhou, R.; Berne, B. J. *J. Phys. Chem. B* **2007**, *111*, 5405−5410.
(48) Liu, B.; Li, X.; Li, B.; Xu, B.; Zhao, Y. *Nano Lett.* **2009**, *9*, 1386−1394.
(49) Yang, Y.; Li, X.; Jiang, J.; Du, H.; Zhao, L.; Zhao, Y. *ACS Nano* **2010**, *4*, 5755−5762.
(50) Liu, P.; Huang, X.; Zhou, R.; Berne, B. J. *Nature* **2005**, *437*, 159−162.